Structural, electrochemical, phosphate-hydrolysis, DNA binding and cleavage studies of new macrocyclic binuclear nickel(II) complexes†

Sellamuthu Anbu,[a] Muthusamy Kandaswamy*[a] and Babu Varghese[b]

Received 4th November 2009, Accepted 11th February 2010
First published as an Advance Article on the web 11th March 2010
DOI: 10.1039/b923078e

New macrocyclic binuclear nickel(II) complexes have been synthesized by using the bicompartmental mononuclear complex [NiL] [3,30-((1*E*,7*E*)-3,6-dioxa-2,7-diazaocta-1,7-diene-1,8-diyl)bis(3-formyl-5-methyl-2-diolato)nickel(II)] with various diamines like 1,2-bis(aminooxy)ethane (L^1), 1,2-diamino ethane (L^2), 1,3-diamino propane (L^3), 1,4-diamino butane (L^4), 1,2-diamino benzene (L^5), and 1,8-diamino naphthalene (L^6). The complexes were characterized by elemental analysis and spectroscopic methods. The molecular structures of the symmetrical binuclear complex $[Ni_2L^1(H_2O)_4](ClO_4)_2$ (**1**) and unsymmetrical binuclear complex $[Ni_2L^3(H_2O)_4](ClO_4)_2{\cdot}(H_2O)_4$ (**3**) were determined by single-crystal X-ray diffraction. The geometry around both the nickel(II) ions in each molecule is a slightly distorted octahedral. The distance between the Ni $\cdots$ Ni centers for complex **1** is 3.039 Å and for complex **3** is 3.059 Å. The influence of the coordination geometry and the ring size of the binucleating ligands on the electronic, redox, phosphate hydrolysis, DNA binding and cleavage properties have been studied. Electrochemical studies of the complexes show two quasi-reversible one electron reduction processes between −0.49 to −1.69 V. The reduction potential of the binuclear Ni(II) complexes shifts towards anodically upon increasing the macrocyclic ring size. The observed first order rate constant values for the hydrolysis of 4-nitrophenyl phosphate reaction are in the range from 8.69×10^{-3} to 1.85×10^{-2} s^{-1}. The complexes show good binding propensity to calf thymus DNA giving binding constant values in the range from 1.4×10^4 to 17.5×10^4 M^{-1}. The absorption, fluorescence and CD spectral data suggests that the complexes are strongly interacting with DNA. These complexes display hydrolytic cleavage of supercoiled pBR322DNA in the presence of H_2O_2 at pH 7.2 and 37 °C. The hydrolytic cleavage of DNA by the complexes is supported by the evidence from free radical quenching and T4 ligase ligation. The pseudo-Michaelis–Menten kinetic parameters $k_{cat} = 1.27 \pm 0.4$ h^{-1} and $K_M = 7.7 \times 10^{-2}$ M for naphthalene diimine containing macrocyclic binuclear nickel(II) complex, (**6**) were obtained.

Introduction

Nickel(II) complexes of a macrocyclic ligand containing mixed donors have attracted much attention because they are used as a model for nickel centred enzymes[1–4] such as bifunctional carbon monoxide dehydrogenase/acetyl-CoA synthase, nickel containing superoxide dismutase, urease and phosphatase. Metal ion mediated hydrolysis of phosphate esters by metallonuclease enzymes is therefore a common catalytic pathway in nucleic acid biochemistry.[5] It was reported that the hexacoordinate dinuclear Ni(II) complexes are more active catalysts for phosphate hydrolysis.[6] Along this line, lots of nickel(II) complexes synthesized and their interactions with DNA have been studied.[7–11] Compared with the number of studies dealing with mononuclear complexes, relatively few studies on binuclear complexes[12] have been reported to date. So, the enhancement of DNA cleavage activity for binuclear complexes[13,14] stimulates to design and synthesize binuclear Ni(II) complexes to evaluate and understand the factors on the DNA-binding properties. Very recently, we have reported the catalytic, nuclease activities of macrocyclic binuclear Cu(II) analogues.[15] With this in view, the new symmetrical and a series of unsymmetrical macrocyclic binuclear Ni(II) complexes have been prepared (Scheme 1) and crystal structure reported.[16] One compartment of the macrocyclic ligand size is fixed by O-alkyl oxime moiety and other compartment of the macrocyclic ligand ring size is modified by using various alkyl and aromatic diamines.

Result and discussion

General properties

The positive ion FAB mass spectrum of the symmetrical binuclear nickel(II) complex $[Ni_2L^1(H_2O)_4](ClO_4)_2$ (**1**) showed a peak at

[a]*Department of Inorganic Chemistry, University of Madras, Guindy Campus, Chennai, 600 025, India. E-mail: mkands@yahoo.com; Fax: +91-44-22300488*

[b]*Sophisticated Analytical Instruments Facility, Indian Institute of Technology, Chennai, 600 036, India*

† Electronic supplementary information (ESI) available: The crystal packing of the macrocyclic binuclear Ni(II) complex **1** (Fig. S1), cyclic voltammograms of complexes **1**, **5** and **2**, **3** and **4** (at anodic potentials) (Fig. S2, S3 and S4, respectively), the pH dependence plot for the binuclear Ni(II) complexes on phosphate hydrolysis reaction (Fig. S5), The DNA binding plots of complexes **1**, **3** and **6** (Fig. S6), the effect of addition of complexes **1**, **3** and **6** on the emission intensity of CT DNA-bound ethidium bromide (Fig. S7), gel electrophoresis diagrams (Fig. S8, S9 and S10). CCDC reference number 710629. For ESI and crystallographic data in CIF or other electronic format see DOI: 10.1039/b923078e

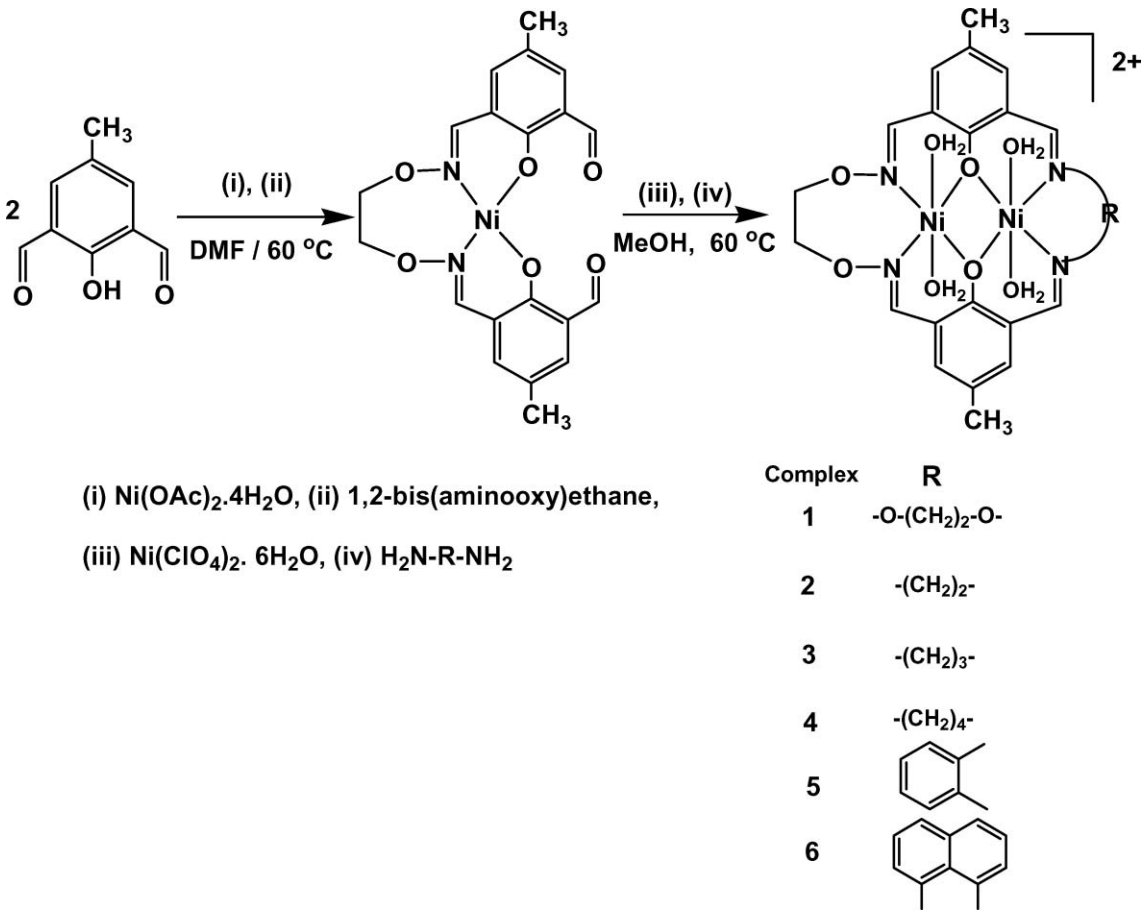

Scheme 1 Synthesis of mono and binuclear Ni(II) complexes.

m/z = 767.39, due to the formation of $[L^{1} + 2Ni + ClO_4]^{+}$ ion. Similarly a series of unsymmetrical binuclear nickel(II) complexes $[Ni_2L^{2-6}(H_2O)_4](ClO_4)_2.(H_2O)_4$ showed a peak at m/z = 866.24 (**2**), 781.42 (**3**), 795.41 (**4**), 815.17 (**5**) and 865.12 (**6**) corresponding to the $[L^{2-6} + 2Ni + ClO_4]^{+}$ ion. The positive ion FAB mass spectral data and elemental analysis are consistent with the proposed formula of all the binuclear Ni(II) complexes. The absorption spectra of all the complexes in CH_3CN, displayed three bands over the range 500–900 nm. These are the characteristic of Ni^{2+} in the six coordination environment.[17,18] These are assigned to the $^3A_{2g} \rightarrow {}^3T_{1g}(P)$, $^3T_{1g}(F)$ and $^3T_{2g}(F)$ transitions, respectively.[19]

Description of the complex molecular structure

Complex **1** (Fig. 1) crystallizes in a monoclinic system with space group $P2_1/n$. Half of the molecule forms the asymmetric unit. The two halves of the molecule are related through center of inversion. The nickel atom(s) have distorted octahedral geometry with approximate square planar base (N1 N2 O3 O3_1, symm_1: $-x, -y, -z$) and fifth and sixth coordination sites are occupied by two water molecules. The ligand bite angles with metal are 88.53° and 88.19°. The distance between Ni···Ni centres was found to be 3.039 Å. Crystallographic data, the list of selected bond lengths, angles and hydrogen bonds are given in the Tables 1 and 2. The packing of the molecule is stabilized through three dimensional OH···O hydrogen bonds mediated through perchlorate anions

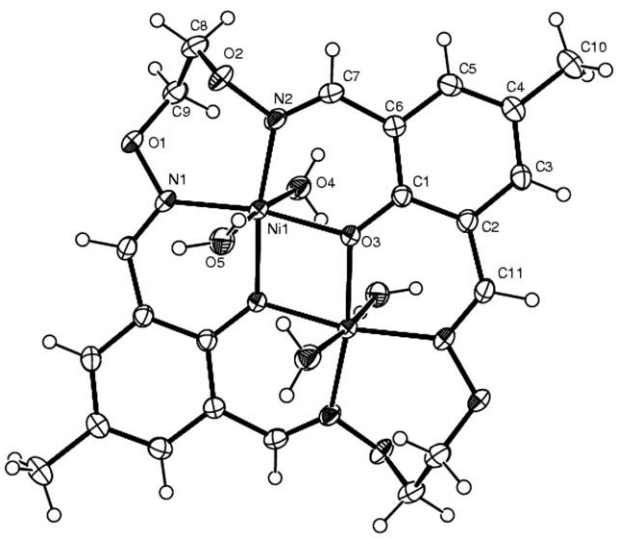

Fig. 1 ORTEP diagram of $[Ni_2L^1(H_2O)_4](ClO_4)_2$ (**1**) Only asymmetric unit is labelled. Displacement ellipsoids are drawn at the 50% probability level. The perchlorate anions are omitted for the sake of clarity.

(ESI Fig. S1).† The *trans* angles at the Ni(II) centres are deviated from 180°, ranging from 170.04(6) to 174.18(6). All other angles subtended at Ni(II) centres are deviated from 90°, ranging from 86.78 (6) to 100.91 (6), which indicates geometry around Ni(II)

Table 1 Crystallographic data for Ni(II) complex **1**

Parameters	Ni_2L^1 (**1**)
Empirical formula	$C_{22}H_{30}Cl_2N_4Ni_2O_{18}$
Formula weight	826.82
T/K	293(2)
λ/Å	0.71069
Crystal system	Monoclinic
Space group	$P2_1/n$
a/Å	8.978(2)
b/Å	12.042(2)
c/Å	14.186(2)
α/°	90
β/°	90.981
γ/°	90
V/Å^3	1533.5(5)
Z	2
D_{calcd}/Mg m^{-3}	1.791
μ/mm^{-1}	1.491
Crystal size/mm	0.25 × 0.20 × 0.16
θ range for data collection/°	2.22 to 32.28
Max. and min. transmission	0.754 and 0.652
Data/restraints/parameters	6545/7/254
Final R indices [$I > 2\sigma(I)$]	$R_1 = 0.0415$
R indices (all data)	w$R_2 = 0.1120$
Largest diffraction peak and hole/e A^{-3}	1.322 and −1.039

Table 2 Selected bond lengths (Å) and angles (°) for the Ni(II) ion environment of **1**

N1–Ni1 2.0370(16)	Ni1–O3–Ni1′ 97.62(5)
N2–Ni1 1.9849(15)	Ni1–O3–Ni1′ 97.62(5)
O3–Ni1 2.0058(12)	N2–Ni1–O3 88.19(6)
O3′–Ni1 2.0328(13)	N2–Ni1–N1 100.91(6)
O4–Ni1 2.0951(15)	O3–Ni1–O4 86.78(6)
O5–Ni1 2.1682(15)	O3–Ni1–N1 170.04(6)
Ni1–Ni1′ 3.039)	O4–Ni1–O5 174.18(6)
O4–H4A–O6 0.850(9) 1.976(12) 2.818(3) 171(3)	
O4–H4B–O5 0.853(10) 2.010(14) 2.834(2) 162(3)	
O5–H5B–O1 0.846(10) 2.215(17) 3.009(2) 156(3)	

are more distorted than the geometry around Ni(II) centres in unsymmetrical macrocyclic Ni(II) analogue[17] (**3**). Fig. 2 shows the molecular structure of the unsymmetrical macrocyclic binuclear Ni(II) complex $[Ni_2L^3(H_2O)_4](ClO_4)_2\cdot(H_2O)_4$ (**3**). The molecule is discrete binuclear species in which each nickel(II) ions are in slightly distorted octahedral. The Ni···Ni distance was found to be 3.059 Å.

Electrochemistry

The cyclic voltammogram of binuclear Ni(II) complexes **1–6** were measured in CH_3CN from the potential region +1.0 to −1.67 and

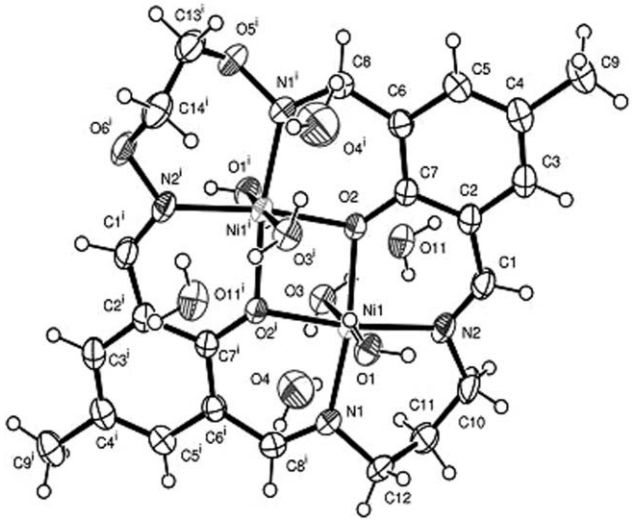

Fig. 2 ORTEP diagram of $[Ni_2L^3(H_2O)_4](ClO_4)_2\cdot(H_2O)_4$ (**3**) The unit cell content of the title compound, showing the atomic numbering scheme. Displacement ellipsoids are drawn at the 50% probability level. The perchlorate anions are omitted for the sake of clarity.

the electrochemical data are summarized in Table 3. The complex **1** showed two *quasi*-reversible reduction waves ($E^1_{1/2} = -0.49$ V and $E^2_{1/2} = -1.30$ V *vs.* Ag/AgCl) in the cathodic region (ESI, Fig. S2).† The complexes **2** to **6** also show two *quasi*-reversible reduction waves (Fig. 3 and ESI, Fig. S3)† in the potential ranges $E^1_{pc} = -1.01$ to −1.26 V and $E^2_{pc} = -1.55$ to −1.67 V. Coulometric experiments by potentiostatic exhaustive electrolysis performed at 100 mV more negative to the first reduction wave consumed approximately one electron ($n = 0.95$) per complex allowing to

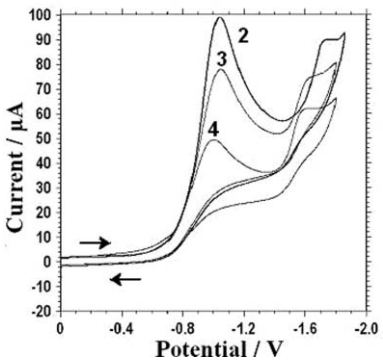

Fig. 3 Cyclic voltammograms of Ni(II) complexes **2**, **3** and **4**.

Table 3 Electrochemical data of binuclear Ni(II) complexes

	Reduction process								Oxidation process				
	E^1_{pc}/V	E^1_{pa}/V	$E^1_{1/2}$/V	ΔE^1/mV	E^2_{pc}/V	E^2_{pa}/V	$E^2_{1/2}$/V	ΔE^2/mV	E^1_{pa}/V	E^2_{pa}/V	E^2_{pc}/V	$E^2_{1/2}$/V	ΔE^2/V
1	−0.56	−0.42	−0.49	140	−1.40	−1.2	−1.30	200	+0.68	+1.02	—	—	—
2	−1.05	−0.83	−0.94	220	−1.67	−1.55	−1.61	120	+0.24	+0.58	+0.38	+0.48	200
3	−1.03	−0.81	−0.92	210	−1.60	−1.50	−1.53	100	+0.22	+0.59	+0.40	+0.50	190
4	−1.01	−0.81	−0.91	200	−1.55	−1.46	−1.50	090	+0.21	+0.62	+0.44	+0.53	180
5	−1.26	−1.16	−1.21	100	−1.63	−1.57	−1.63	110	+0.26	+0.56	+0.43	+0.49	140
6	−1.19	−1.10	−1.14	090	−1.58	−1.49	−1.53	090	+0.23	+0.54	+0.41	+0.47	130

attribute this quasi reversible signal to the $Ni_2^{II,II}/Ni_2^{II,I}$ redox couple. The second quasi-reversible wave can be attributed to the formation of the $Ni_2^{I,I}$ species from the reduction of $Ni_2^{II,I}$. Both the mixed-valence $Ni_2^{II,I}$ and $Ni_2^{I,I}$ species are stable at the time scale of the CV (0.05 V s^{-1}). Based on these observations, it is reasonable to suggest that the reduction process may involve the stepwise redox processes depicted.

$$Ni^{II}Ni^{II} \rightleftharpoons Ni^{II}Ni^{I} \rightleftharpoons Ni^{I}Ni^{I} \quad (1)$$

The effect of scan rate (υ) on the cyclic voltammetric response was examined in a wide scan rate range from 50 to 300 mV s^{-1}. ΔE values are greater than 59/n mV (of the order of 100 mV) and increases with scan rate (ESI, Fig. S2 and S3).† The cathodic and anodic peak current ratio is greater than unity. The nature of the wave shape broadens as this scan rate increases. This indicates that the redox processes are quasi-reversible in nature. Two different reduction and oxidation waves of all the Ni(II) complexes may be due to Ni(II) ions present in two different compartments as well as electrostatic effects arises during redox processes. When the first Ni(II) ion is getting reduced then the charge of the complex decreases from +2 to +1. Therefore, the second Ni(II) ion reduced at higher negative potentials. It was reported[20] that the metal ion in oxime moiety reduces at less negative potential than the metal ion in imine[21a] moiety. We have reported[15] that the influence of more electronegative oxygen atoms in the alkyl oxime moiety makes the Cu(II) ion to reduce at less negative reduction potentials. The donor nature of alkyl group in the alkyl imine[21b] moiety increases the electron density around the Cu(II) ion and makes to reduce at higher negative potentials. It is noticed that geometry around both the Cu(II) ions in unsymmetrical Cu(II) analogues is square pyramid. Presently, geometry around both the Ni(II) ions in alkyl oxime and imine moiety is octahedral. Like Cu(II) complexes, the Ni(II) ion in oxime moiety may reduces first than the Ni(II) ion in imine moiety. As the chain length of the alkylimine compartment increases, the entire macrocyclic ring becomes more flexible. The distortion around the geometry also increases. It has been suggested[22–24] that reduction of electron density on the metal ions and distortion in geometry favours the reduction process (Ni^{II}/Ni^{I}) at less negative potentials, as observed in the complex of ligand L^4 relative to ligand L^2. As the size of the macrocycle is increased, shifting of both first and second reduction potentials towards anodic is observed for the binuclear nickel(II) complexes. Complexes containing aromatic group (**5** and **6**) in the imine nitrogen compartment get reduced at higher potential than the other complexes containing alkyl group in the imine nitrogen compartment. The higher reduction potential can be attributed due to the greater planarity and electronic properties those are associated with aromatic rings.[24]

In the positive potential region complex (**1**) showed two irreversible oxidation waves (E^1_{pa} = +0.68 V and E^2_{pa} = +1.02 V). Whereas, complexes **2–6** showed an irreversible (E^1_{pa} = +0.21 V to +0.26 V) followed by a quasi-reversible ($E^2_{1/2}$ = +0.48 V to +0.53 V *vs.* Ag/AgCl) oxidation waves (ESI, Fig. S4).† Controlled potential electrolysis experiment indicates that the two oxidation peaks are associated with stepwise oxidation process at metal center.

$$Ni^{II}Ni^{II} \rightarrow Ni^{II}Ni^{III} \rightleftharpoons Ni^{III}Ni^{III} \quad (2)$$

It must be noted that the symmetrical macrocyclic ligand containing electronegative oxygen atoms of the oxyime group causes a destabilization of the oxidized form of the complex and therefore the irreversibility of the anodic electrochemical responses were observed. There is slight anodic shift was observed as the number of methylene groups (chain length) increases in the imine compartment of unsymmetrical macrocyclic Ni(II) analogues **2–4**. This can be due to the presence of the azomethine group in one compartment affects electron-transfer potentials[25] leading to a strong negative shift in the cathodic waves and slight positive shift is observed for the oxidation waves.

Phosphate hydrolysis

Many hydrolytic processes in enzyme-catalysis involve metal ions that are assumed to activate a water molecule which is more easily to form hydroxyl group as a nucleophilic group in reaction system.[26] Presently, all the binuclear Ni(II) complexes possesses in its structure a potential nucleophile constituted by the metal coordinated water molecule, and their catalytic activities on hydrolysis of 4-nitrophenyl phosphate (4-NPP) was investigated spectrophotometrically by following the absorption increase at 400 nm due to the formation of 4-nitrophenolate ion over time. The effect of pH on the rate of reaction was determined and correlated with the pK_a of coordinated water in **1**. The pH dependence plot for the binuclear Ni(II) complexes on phosphate hydrolysis reaction showed a pH-independent rate above 8.5 and a range below this pH where the initial rate of hydrolysis increases with pH (ESI, Fig. S5).† The derived sigmoidal pH-rate profiles are characteristic of a kinetic process controlled by an acid–base equilibrium and exhibit inflection points corresponding to the pK_a value is 7.89 for one of the coordinated water molecule. This indicates that the $[Ni_2(L)(H_2O)_3(OH)]$ complex is the reactive species. The Ni(II)-bound OH^- acts as a nucleophile to attack the phosphate atom of the 4-NPP and hydrolysis takes place. Since the substrate concentration was essentially constant during the measurement, the initial first order rate constant (k_{obs}) was measured at different concentrations of the catalyst at pH 7.6 and 25 ± 0.1 °C. Plots of rate constant (k_{obs}) *vs.* complex concentration are presented in Fig. 4. As can be seen, for all complexes, the rate of 4-NPP cleavage initially increases linearly with the increase of complex concentration but gradually the reaction order in the catalyst concentration deviates from unity. In other words, the reaction exhibits a first order dependence only at low Ni(II) complex concentrations. The k_{obs} value for phosphate hydrolysis reaction by nickel(II) perchlorate hexahydrate salt was found as 2×10^{-13} s^{-1}. This is negligibly small when compare to the k_{obs} value (10^8 times more faster) for binuclear Ni(II) complexes. The first order rate constants k were obtained for the Ni(II) complexes, from Lineweaver–Burk plot, *i.e.*, $1/V_0$ *vs.* 1/[4-NPP] by changing concentration of substrate (Fig. 5) and the results of calculation are summarized in Table 4. These values are comparable to the constants reported by Yamaguchi *et al.*[6] for the hydrolytic cleavage of 4-NPP by binuclear Ni(II) complexes. From Table 4, it can be seen that the catalytic activity of the complexes (**2**, **3** and **4**) are found to increase as the macrocyclic ring size increases, because of the intrinsic flexibility of the ligand makes the geometry around metal ion is more distorted. The aromatic diimines containing complexes (**5** and **6**) are also shows remarkable catalytic activity. It is noted that

Table 4 Rate constants for phosphate hydrolysis and DNA binding parameters of the binuclear Ni(II) complexes

Complexes	4-NPP Hydrolysis k/s^{-1}	10^4 K_b[a]	$10^5 K_{app}$[b]	CD $\Delta\lambda_{max} + \Delta\varepsilon$[c]
1	1.85×10^{-2}	3.1	4.2	−3 (11)
2	8.69×10^{-3}	—	—	−2 (1)
3	1.20×10^{-2}	1.4	3.7	−2 (3)
4	1.73×10^{-2}	—	—	−3 (4)
5	1.68×10^{-2}	—	—	−3 (10)
6	1.70×10^{-2}	17.5	12.2	−4 (11)

[a] Binding constants (M^{-1}) were determined by absorption spectrophotometric titration. [b] Apparent binding constants (M^{-1}) were determined by fluorescence spectrophotometric method. [c] $\Delta\lambda_{max}$ is the shift in nm of the positive DNA CD band at 274 nm. $\Delta\varepsilon$ (the value in parentheses) is the difference between the maximum ellipticity (in °) observed for the positive CD band in the spectrum of a 2 : 1 reaction mixture, and the ellipticity observed at the same wavelength in the spectrum of free CT DNA.

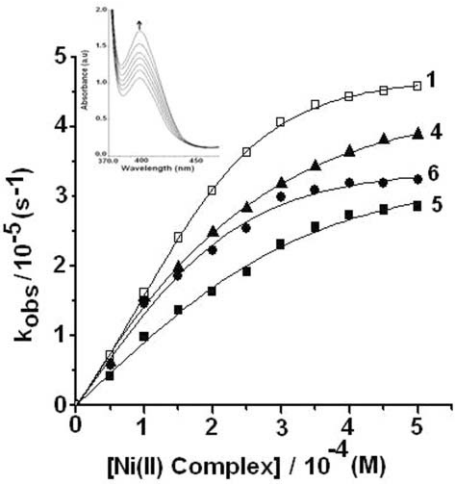

Fig. 4 Dependence of the reaction rate on the concentration of **1**–**4** for the 4-NPP hydrolysis at pH 7.60 and 25 ± 0.1 °C. Conditions: [4-NPP] = 5.0×10^{-5} M, [Ni_2 complex] = 5.0×10^{-5} to 5.0×10^{-4}, [buffers] = 50 mM, $I = 0.1$ M ($NaClO_4$). Inset shows the hydrolysis of 4-NPP by the binuclear nickel(II) complex **4**.

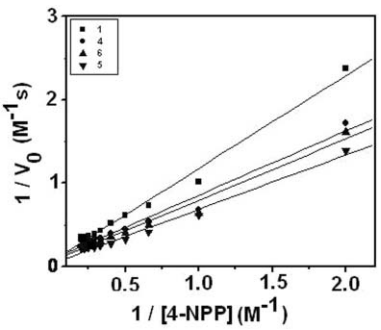

Fig. 5 Lineweaver–Burk plot for the 4-NPP hydrolysis by complexes **1**, **4**, **5** and **6**.

the oxime containing symmetrical Ni(II) complex **1** display higher catalytic activity than the unsymmetrical Ni(II) analogues **2**–**6**. This may be due to more electronegative oxygen atom of the oxime nitrogen atoms of both the compartments, which reduces the electron density around metal ion and favors easy deprotonation of metal coordinated water molecule. It has been assumed that the geometry around the Ni(II) ions and the intermetallic distance are the two key factors that determine the catalytic activity of the complexes. The distance between the Ni···Ni centres is smaller (3.039 Å (**1**)) than the unsymmetrical Ni(II) analogues. The Ni···Ni distance also influence the rate of phosphate hydrolysis reaction. The first order rate values of the unsymmetrical binuclear Ni(II) complexes were found to increase as the macrocyclic ring size increases. It is evident from the literature,[24,27–29] that the first order rate values for the more distorted complexes are higher than those of the less-distorted complexes.

DNA binding and cleavage properties

Absorption spectral studies. Absorption spectral titration experiment is used to monitor the interaction of Ni(II) complexes **1**, **3** and **6** with CT DNA (Fig. 6, Table 4). A complex generally shows hypochromism and a red shift[30] (bathochromism) of the absorption band when it binds to DNA through intercalation, resulting in a strong stacking interaction between the aromatic chromophore of the ligand and the base pairs of the DNA. The extent of hypochromism[31] gives a measure of the strength of an intercalative binding. The observed trend in hypochromism among the present complexes follows the order complexes **6** > **1** > **3**. The binding constants K_B of the Ni(II) complexes to CT DNA were determined by monitoring the changes of absorbance with increasing concentration of DNA. The binding constant K_B (ESI, Fig. S6)† of complexes **1**, **3** and **6** are calculated as 3.1×10^4, 1.4×10^4 and 17.5×10^4 M^{-1}, respectively. The better binding of the complex **6** than the complexes **1** and **3** may be due to the co-planarity of the naphthalene ring system in the macrocyclic ring. It is expected to be stacked between the base pairs upon the interaction of the complex with DNA.[32] Structurally, the ligand **6** should provide aromatic moiety to overlap with the stacking base pairs of the DNA helix by intercalation which results in hypochromism and bathochromism. The increasing aromatic moiety in macrocyclic ligands of the nickel(II) complexes, that facilitates its potential intercalative binding, while complexes **1** and **3** may prefer electrostatic interaction.

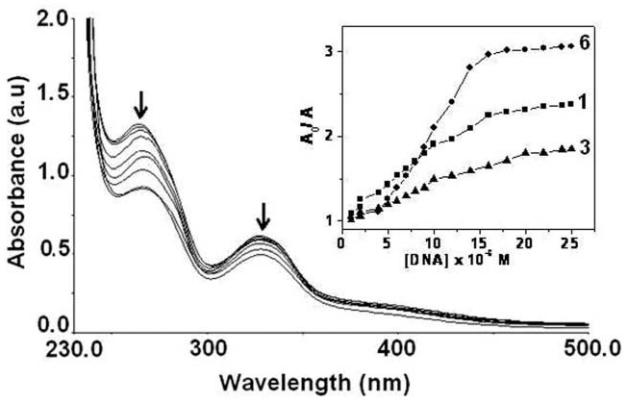

Fig. 6 Absorption spectra of complex **1** (1×10^{-5} M) in the absence (line-a) and presence of increasing amounts of CT-DNA (0-2.5×10^{-3} M) at room temperature in 50 mM Tris-HCl/NaCl buffer (pH = 7.5). Arrow shows the absorbance changing upon increasing DNA concentrations. Insets shows the saturation in absorption intensity hypochromism is indicated by the plot of A_0/A *vs.* [DNA].

Fluorescence spectral studies. The fluorescence spectral method is used to study the relative binding of these complexes to CT-DNA. The emission intensity of ethidium bromide (EB) is used as a spectral probe.[33] The fluorescence of EB increases after intercalating into DNA. If the metal complex intercalates into DNA, it leads to a decrease in the binding sites of DNA available for EB resulting in decrease in the fluorescence intensity of the EB-DNA system.[34] Nickel(II) perchlorate hexahydrate salt and complexes **1**, **3** and **6** were added to DNA pretreated with EB. No significant quenching was observed in fluorescence of EB bound DNA while adding increasing amounts of nickel(II) perchlorate hexahydrate (ESI, Fig S7).† Complexes **1**, **3** and **6** cause an appreciable reduction in fluorescence intensity, (Fig. 7) indicating that complexes competes with EB to bind with DNA.[35] The fluorescence quenching curve of DNA-bound EB by complex **6** is in good agreement with the linear Stern–Volmer equation. In the linear fit plot of I_0/I *vs.* [complex]/[DNA], K is given by the ratio of the slope to intercept. (I_0 is the emission intensity of EB-DNA in the absence of complex; I is the emission intensity of EB-DNA in the presence of complex) The K value of the complexes **1**, **3** and **6** were calculated as 6.61($R = 0.985$), 5.01($R = 0.991$) and 12.6($R = 0.989$), respectively. The concentrations of the complexes are taken for observing 50% reduction of emission intensity of EB.[22] From the data in the ESI, Fig. S7,† it is also know that 50% of EB molecules were replaced from DNA-bound EB at a concentration ratio of [Ni_2complex]/[EB] = K_1. The K_1 value of the complexes **1**, **3** and **6** were found as 23.8, 27.0 and 8.19, respectively. By taking a DNA binding constant 1.0×10^7 M^{-1} for EB[36] an apparent DNA binding constant K_{app} of the complexes (4.2×10^5 (**1**), 3.7×10^5 (**3**) and 1.22×10^6 (**6**) M^{-1}) were derived from the equation (K_b(EB)/K_1). The K_{app} values imply that the complex **6** can strongly interact with DNA and protected by DNA efficiently. The intercalation of 4-methylphenol group and also the hydrophobic property of the rigid macrocyclic ligands also facilitate the DNA binding.[36] The greater K_{app} value for complex **6** than the complexes **1** and **3** may be due to the presence of more aromatic moiety, which enhances the binding propensity of the molecule to DNA. The DNA binding constants K_{app} of the complexes were obtained from EB displacement (indirect method) are different from those obtained (K_B) from absorption spectral method (direct method). The same was reported for Co^{3+} and Ru^{2+} complexes.[31,37] This difference between the two sets of binding constants may be caused by the different spectroscopy and different calculation method.

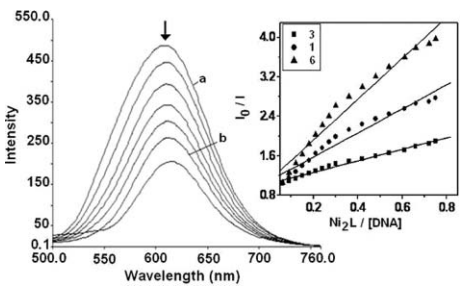

Fig. 7 Emission spectrum of EB bound to DNA in the presence of ([EB] = 3.3 μM, [DNA] = 40 μM, [complex] = 0-25 μM, λ_{ex} = 430 nm). Arrow shows the absorbance changing upon increasing Ni(II) complex (**6**) concentrations. Inset shows the plots of emission intensity I_o/I *vs.* [DNA]/[Ni(II) complex].

Viscosity measurements. In order to clarifying the binding mode of Ni(II) complexes **1**, **3**, **6** with DNA, viscosity of DNA solutions containing varying amount of added complexes were measured. A classical intercalation model demands that the DNA helix lengthens as base pairs are separated to accommodate the binding ligand, leading to the increase of DNA viscosity.[38] The effects of complexes **1**, **3**, **6** and EB on the viscosity of rod-like DNA, are shown in Fig. 8. EB, a well known DNA intercalator, gave rise to a strong change in DNA viscosity upon complexation. Complexes **1** and **3** binds by electrostatic intercalations only, exerted essentially no such effect. After increasing the amounts of **6** the relative viscosity of DNA increases steadily, similar to EB. The increase in relative viscosity, expected to correlate with the compound's DNA-intercalating potential, followed the order EB > **6** > **1** > **3**. These results suggest that complex **6** can bind to DNA through intercalation, due to the presence of naphthalene ring system in one compartment of the ligand.

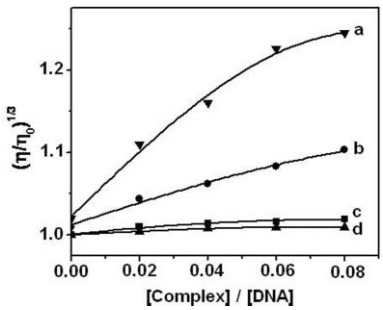

Fig. 8 Effect of increasing amounts of EB (a), Ni(II) complexes **1**, **3** and **6** (b, c and d, respectively) on the relative viscosity of calf thymus DNA at 25 (±0.1) °C. The total concentration of DNA is 0.5 mM.

CD spectral studies. Circular dichorism (CD) is a useful method to access whether nucleic acids undergo conformational changes as a result of complex formation or changes in the environment.[39] The UV circular dichoric spectrum of CT DNA exhibits positive band at 272 nm (UV: λ_{max} 260 nm) due to base stacking and negative band at 239 nm due to helicity of B-DNA.[40] It was reported[30] that the change in ellipticity and shifting to higher energy of the positive CD signals are due to intercalative mode of binding. Incubation of the DNA with the complexes **1–6**, induced considerable changes in CD spectrum (Fig. 9). At a [Ni_2complex] : CT DNA ratio of 2 : 1 all nickel(II) complexes produced shifts to higher energy for the positive CD signal as well as an enhancement of CD ellipticity at 272 nm. Examination of Table 4 shows that the magnitude of the increases in elipticity at 272 nm increase in the following order. **2** < **3** < **4** < **1** < **5** < **6**. The result reveals that the changes induced by **5** and **6** are more significant than those by **1–4**, which suggests that **6** have higher affinity for CT DNA than the complexes **1–4** does. It is reasonable to suggest that the higher affinity of complexes **5** and **6** with CT DNA due to presence of aromatic moiety in the one compartment of the macrocyclic ligand, which enhances the interaction, while the complexes **1–4** induced only slight conformational changes in DNA may be due to presence of aliphatic moiety in both the compartments.

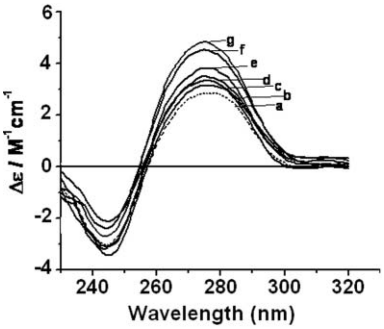

Fig. 9 CD spectra recorded over the wavelength range 230–320 nm for solutions containing 2 : 1 ratio of CT-DNA (200 μM) and binuclear Ni(II) complexes **1–6** (100 μM). (a = CT DNA, b = **2** + DNA, c = **3** + DNA, d = **4** + DNA, e = **1** +DNA, f = **5** + DNA and g = **6** + DNA).

DNA cleavage activity. The interaction of complexes **2**, **5** and **6** with pBR322 DNA was studied by monitoring the conversion of circular supercoiled DNA (Form I) to nicked (Form II) and linear (Form III) DNA. The amount of strand scission was assessed by agarose gel electrophoresis. Fig. 10 shows the electrophoretic pattern of plasmid DNA treated with complexes **2**, **5** and **6** (30–50 μM) in the presence of H_2O_2 (40 μM). Control experiments suggest that untreated DNA and DNA incubated with either complex or peroxide alone did not show any significant DNA cleavage (lanes 1–5). At 50 μM concentration of the binuclear complexes, the cleavage is found to be significant, as is seen from the formation of nicked circular (form II) and linear form (form III) in lanes 6–8. The cleavage mechanism of pBR322 DNA induced by complexes **3** and **6** were investigated (ESI, Fig. S8)† and clarified in the presence of hydroxyl radical scavenger 0.4 M DMSO (lanes 2 and 4), superoxide quencher SOD (4 units) (lanes 3 and 5) and EDTA as a chelating agent under aerobic conditions.[41] As shown in the ESI, Fig. S8,† the DNA cleavage mechanism by complexes **3** and **6** are shown as follows: both DMSO and SOD (lanes 2–5) do not alter DNA cleavage activity, these rules out the possibility of cleavage by hydroxyl radical and superoxide, respectively. The EDTA (lanes 6 and 7) efficiently inhibit the DNA cleavage activity of the Ni(II) complexes in a similar way to that for nuclease.[36] In order to ascertain the hydrolytic cleavage mechanism, the cleavage studies were carried out under anaerobic conditions as shown in the ESI, Fig. S9.† Under anaerobic conditions, the binuclear Ni(II) complex display considerable cleavage (lanes 1–5). This fact implies that the DNA cleavage reaction by the binuclear Ni(II)/H_2O_2 system should be due to hydrolytic mechanism. To confirm the hydrolytic cleavage, the linear form obtained from the cleavage of SC DNA was reacted with T4 ligase enzyme (ESI, Fig. S10)† and observed the complete conversion of the linear DNA to its original form.[42] It is well known that in DNA hydrolytic cleavage 3′-OH and 5′-OPO_3 (5′-OH and 3′-OPO_3) fragments remain intact and that these fragments can be enzymatically ligated.[43] The linear DNA was recovered from low melting point gel by cutting off the gel fragment and subjecting to overnight ligation reaction with T4 ligase. The electrophoretic results (ESI, Fig. S10)† show that the linear DNA fragments cleaved by **5** and **6** can be re-ligated by T4 ligase just like the linear DNA mediated by the natural enzyme EcoRI.[44] The kinetic aspects of the hydrolytic DNA cleavage (Fig. 11) by **6** is found to vary exponentially with incubation time and it follows pseudo-first order kinetics. Kinetic plots showing the formation of nicked circular (NC) DNA, linear DNA and the degradation of SC DNA *vs.* time follow pseudo-first order kinetics and they fit well to a single exponential curve. Under true Michaelis–Menten conditions in which the complex concentration is kept constant at 55 μM and the DNA concentration is varied from 41–180 μM, we are able to obtain the rate constant of 1.27 ± 0.4 h^{-1} using 150 μM SC pBR322 DNA. The linear plot of log (%SC-DNA) *vs.* time (Fig. 12a) from which we have determined the hydrolytic rate constant is shown in Fig. 12b. The pseudo Michaelis–Menten kinetic parameters k_{cat} = 1.27 ± 0.4 h^{-1} and $K_M = 7.7 \times 10^{-2}$ M

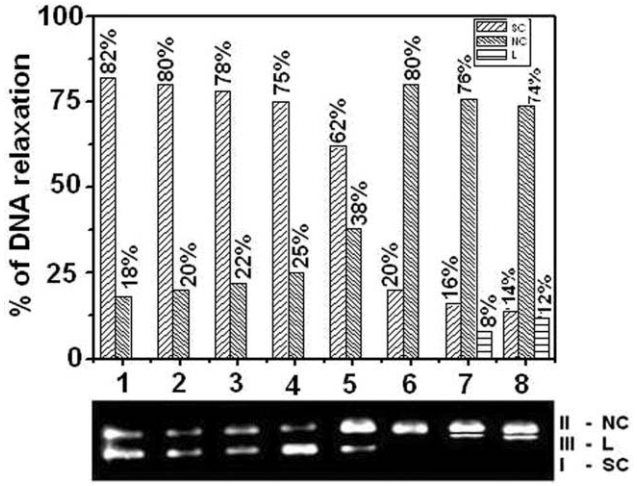

Fig. 10 Cleavage of SC pBR322 DNA (0.2 μg, 33 μM) by Ni(II) complexes **1**, **5** and **6** (30–50 μM) in the presence of H_2O_2 (40 μM) in 50 mM Tris-HCl/NaCl buffer (pH 7.2). Lane 1, DNA control; lane 2, DNA + H_2O_2; lane 3, DNA + **1** (30 μM); lane 4, DNA + H_2O_2 + **5**(30 μM); lane 5, DNA + H_2O_2 + **6** (30 μM); lane 6, DNA + H_2O_2 + **1** (50 μM); lane 7, DNA + H_2O_2 + **5** (50 μM); lane 8, DNA + H_2O_2 + **6** (50 μM).

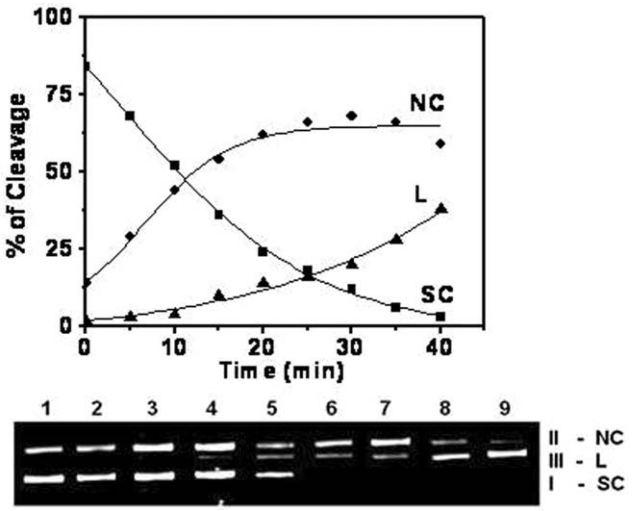

Fig. 11 Cleavage activity of **6** monitored by 0.8% agarose gel electrophoresis, where [DNA] (0.2 μg, 33 μM) by (**6**) 50 μM, and [H_2O_2] 40 μM. Time course measured in 10 mM Tris buffer, pH 7.4, 37 °C, showing the disappearance of supercoiled DNA (I) at (1) 0 min, (2) 5 min, (3) 10 min, (4) 15 min, (5) 20 min, (6) 25 min, (7) 30 min, (8) 35 min (9) 40 min. (Gel image showing supercoiled (Form I), circular relaxed (Form II), linear (Form III) DNA.)

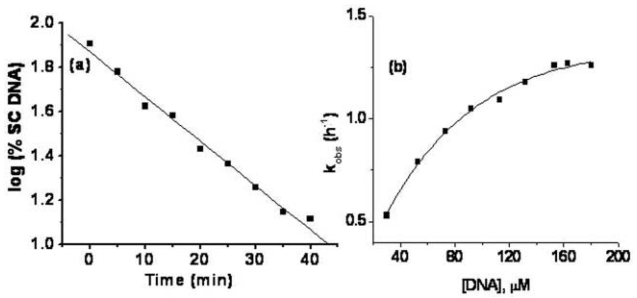

Fig. 12 (a) Plot of log (%SC DNA) *vs.* time for a complex concentration of 50 μM. (b) Saturation kinetics of the cleavage of pBR322 DNA using 50 μM complex **6** with different concentrations of SC DNA (33–183 μM) at 37 °C in 50 mM Tris-HCl/NaCl buffer (pH 7.2).

for complex **6** was calculated. This k_{cat} value of complex **6** is comparable to the DNA hydrolytic rate constant (k_{cat}) value of reported[12,45] Ni(II) complexes.

Experimental

Materials and measurements

2,6-Diformyl-4-methylphenol[46] and 1,2-bis(aminooxy)ethane[47] were prepared by following the literature methods. Tetra(*n*-butyl)ammonium perchlorate (TBAP) was purchased from Fluka and recrystallized from hot methanol. (**Caution!** TBAP is potentially explosive; hence care should be taken in handling the compound.) All the solvents were purified by reported procedures.[48] CT-DNA and pBR322DNA were purchased from Bangalore Genie (India). All other chemicals and solvents were of analytical grade and used as received. Elemental analysis was conducted on a Carlo Erba model 1106 elemental analyzer. FT-IR spectra were obtained on a Perkin Elmer FTIR spectrometer with samples prepared as KBr pellets. UV-vis spectra were recorded using a Perkin Elmer Lambda 35 spectrophotometer operating in the range of 200–1000 nm with quartz cells and ε are given in M^{-1} cm^{-1}. CH11008 Electrochemical analyzer using a three- electrode cell setup comprised of glassy carbon working, platinum wire auxiliary, and saturated Ag/AgCl electrodes. The concentration of the complexes was 10^{-3} M and TBAP (10^{-1} M) was used as the supporting electrolyte.

Synthesis of mononuclear nickel(II) complex

Synthesis of [NiL]. To a solution of 2,6-diformyl-4-methyl phenol (3.0 g; 1.8 mmol) in warm dimethyl formamide (30 mL), 1,2-bis(aminooxy)ethane (0.84 g. 0.9 mmol) (**I**) was added dropwise under constant stirring. Solid $Ni(OAc)_2{\cdot}4H_2O$ (1.8 g; 0.9 mmol) was added and the solution was stirred at 60 °C for 2 h. A greenish yellow colored mononuclear complex [NiL] precipitated. The solid was separated by filtration and washed with isopropyl alcohol and diethyl ether (3.6 g, 44%). $C_{20}H_{18}N_2NiO_6$ (441.32): C 54.46, H 4.11, N 6.35. Found: C 54.42, H 4.06, N 6.32.

Synthesis of binuclear nickel(II) complexes

Synthesis of $[Ni_2L^1(H_2O)_4]2ClO_4$ (1). The binuclear Ni(II) complex **1** was prepared from a general synthetic procedure in which the vigorously stirred suspension of mononuclear complex NiL (0.5 g, 1.13 mmol) in methanol (25 mL), a methanolic solution of $Ni(ClO_4)_2{\cdot}6H_2O$ (0.41 g, 1.13 mmol) was added slowly and the mixture was stirred for 15 min to obtain a clear solution. Then the methanolic solution (5 mL) of 1,2-bis(aminooxy)ethane (0.10 g, 1.13 mmol) was added drop wise to the above solution and refluxed for 3 h. A resulting solid was separated on evaporating the solution at room temperature. Green crystals suitable for X-ray analysis were obtained after several days by slow evaporation of acetonitrile solution (0.62 g 84%). $C_{22}H_{30}Cl_2N_4Ni_2O_{18}$ (627.88): C 42.05, H 4.78, N 8.92. Found: C 42.12, H 4.74, N 8.87. FAB-MS in NBA: *m*/*z*: 767.39 $[L^1 + 2Ni + ClO_4]^+$. FT-IR (KBr, ν/cm^{-1}: 3445 br, 2925 s, 1638 s, 1107 vs, 625 s, 502 w. UV-vis: λ_{max} (CH_3CN)/nm: 952, 742, 560, 328 and 265 (ε/dm^3 mol^{-1} cm^{-1}: 30, 40, 62, 54 000 and 170 000).

Synthesis of $[Ni_2L^2(H_2O)_4]4H_2O{\cdot}2ClO_4$ (2). This complex was prepared by the method used for **1**, using 1,2-diamino ethane in place of compound **I**, offered orange coloured solid (0.73 g, 74%). Elemental analysis data: calcd (%) for $C_{22}H_{38}Cl_2N_4Ni_2O_{20}$ (866.84): C 30.46, H 4.38, N 6.46. Found (%): C 30.41, H 4.44, N 6.38. FAB-MS in NBA: *m*/*z*: 866.24 $[L^2 + 2Ni + ClO_4]^+$. FT-IR (KBr, ν/cm^{-1}: 3428 br, 2921 m, 1625 s, 1343 m, 1087 s, and 623 s. UV-vis: λ_{max} (CH_3CN)/nm: 970, 560, 426, 375 and 263 (ε/dm^3 mol^{-1} cm^{-1}: 30, 180, 2820, 58 000 and 33 000).

Synthesis of $[Ni_2L^3(H_2O)_4]4H_2O{\cdot}2ClO_4$ (3). This complex was prepared by the method used for **1**, using 1,3-diamino propane in place of compound **I**, offered green coloured crystals (0.75 g, 75%). Elemental analysis data: calcd (%) for $C_{23}H_{40}Cl_2N_4Ni_2O_{20}$ (880.87): C 31.33, H 4.54, N 6.36. Found (%): C 31.41, H 4.62, N 6.41. FAB-MS in NBA: *m*/*z*: 781.42 $[L^3 + 2Ni + ClO_4]^+$. FT-IR (KBr, ν/cm^{-1}: 3431 br, 2922 m, 1628 s, 1342 m, 1088 s, and 624 s. UV-vis: λ_{max} (CH_3CN)/nm: 975, 566, 432, 380 and 265 (ε/dm^3 mol^{-1} cm^{-1}: 33, 182, 2830, 58 500 and 35 000).

Synthesis of $[Ni_2L^4(H_2O)_4]4H_2O{\cdot}2ClO_4$ (4). This complex was prepared by the method used for **1**, using 1,4-diamino butane in place of compound **I** offered pale green coloured solid (0.76 g, 75%). Elemental analysis data: calcd (%) for $C_{24}H_{42}Cl_2N_4Ni_2O_{20}$ (894.9): C 32.18, H 4.69, N 6.26. Found (%): C 32.24, H 4.72, N 6.32. FAB-MS in NBA: *m*/*z*: 795.41 $[L^4 + 2Ni + ClO_4]^+$. FT-IR (KBr,ν/cm^{-1}: 3432 br, 2925 m, 1630 s, 1343 m, 1089 s, and 625 s. UV-vis: λ_{max} (CH_3CN)/nm: 976, 569, 440, 383 and 269 (ε/dm^3 mol^{-1} cm^{-1}: 35, 186, 2910, 58 900 and 38 000).

Synthesis of $[Ni_2L^5(H_2O)_4]4H_2O{\cdot}2ClO_4$ (5). This complex was prepared by the method used for **1**, using 1,2-diamino benzene in place of compound **I** offered orange coloured solid (0.70 g, 70%). Elemental analysis data: calcd (%) for $C_{26}H_{34}Cl_2N_4Ni_2O_{18}$ (914.88): C 34.10, H 3.71, N 6.12. Found (%): C 34.21, H 3.68, N 6.18. FAB-MS in NBA: *m*/*z*: 815.17 $[L^5 + 2Ni + ClO_4]^+$. FT-IR (KBr, ν/cm^{-1}: 3435 br, 2921 w, 1635 s, 1342 m, 1087 s, and 625 s. UV-vis: λ_{max} (CH_3CN)/nm: 975, 572, 442, 380 and 266 (ε/dm^3 mol^{-1} cm^{-1}: 32, 182, 2830, 60 500 and 40 000).

Synthesis of $[Ni_2L^6(H_2O)_4]4H_2O{\cdot}2ClO_4$ (6). This complex was prepared by the method used for **1**, using 1,8-diamino naphthalene in place of compound **I** offered green colored solid (0.73 g, 69%). Elemental analysis data: calcd (%) for $C_{30}H_{36}Cl_2N_4Ni_2O_{18}$ (964.94): C 37.31, H 3.73, N 5.80. Found (%): C 37.43, H 3.79, N 5.95. FAB-MS in NBA: *m*/*z*: 865.12 $[L^6 + 2Ni + ClO_4]^+$. FT-IR (KBr, ν/cm^{-1}:

3441 br, 2920 w, 1636 s, 1345 m, 1088 s, and 625 s. UV-vis: λ_{max} (CH_3CN)/nm: 980, 576, 448, 386 and 267 (ε/dm^3 mol^{-1} cm^{-1}: 35, 190, 2780, 61 100 and 39 000).

X-Ray crystallography

Crystals of complexes **1** and **3** were translucent green and cut to suitable size and mounted on Kappa Apex2 CCD diffractometer equipped with graphite monochromated Mo Kα radiation (λ = 0.71073 Å). The intensity data were collected using ω and φ scans with frame width of 0.5°. The frame integration and data reduction were performed using Bruker SAINT-Plus (version 7.06a) software.[49] The multi-scan absorption corrections were applied to the data using SADABS (Bruker 1999)[50] program. Both samples were stable at room temperature. The structures were solved using SIR92 (Altornare *et al.*, 1993).[51] Full-matrix least-squares refinement was performed using SHELXL-97 (Sheldrick, 1997) programs. All the non-hydrogen atoms were refined with anisotropic displacement parameters. All the hydrogen atoms could be located in a difference Fourier map. However, they were relocated at chemically meaningful positions and were given riding model refinement. The refinement of water hydrogen atoms were restrained such that they remain in the vicinity of the respective difference peak.

Phosphate hydrolysis

Kinetic experiments for the hydrolysis of 4-nitrophenyl phosphate were followed spectrophotometrically on a Perkin Elmer UV-spectrophotometer. The effect of pH on the reaction rate for the hydrolysis of 4-NPP promoted by complexes **1–6** was determined over the pH range 3.9–10.5. Reactions were performed using the following conditions: 3 mL of freshly prepared buffer aqueous solution (50 mM, 0.1 mM KCl, buffer: acetato (pH 3.9 and 4.9), MES (pH 6), Bis-Tris propano (pH 7.0, 7.6 and 8.0), CHES (pH 8.94 and 10.52) and 1 mL of 4×10^{-3} M complex solution [acetonitrile–water (2.5% (v/v))] were added to a 1 cm path length at 25 °C.

DNA binding experiments

The DNA binding experiments were performed in Tris-HCl/NaCl buffer (50 mM Tris-HCl/1 mM NaCl buffer, pH 7.5) using dimethyl formamide (DMF) (10%) solution of the complexes **1**, **3** and **6**. The concentration of CT DNA was determined from the absorption intensity at 260 nm with a ε value[52] of 6600 M^{-1} cm^{-1}. Absorption titration experiments were made using different concentration of CT DNA, while keeping the complex concentration as constant. Due correction was made for the absorbance of the CT DNA itself. Samples were equilibrated before recording each spectrum. The intrinsic binding constant, K_b for the complexes **1**, **3** and **6** has been determined from the spectral titration data using the following equation.[53]

$$[DNA]/(\varepsilon_a - \varepsilon_f) = [DNA]/(\varepsilon_b - \varepsilon_f) + 1/K_b(\varepsilon_b - \varepsilon_f) \quad (3)$$

Here, ε_a, ε_f, and ε_b, correspond to A_{obsd}/[Ni(II) complex], the extinction coefficient for the free complex, and the extinction coefficient for the complex in the fully bound form, respectively. The non-linear least-squares analysis was done using Origin Lab, version 6.1.

The fluorescence spectral method using EB as a reference was used to determine the relative DNA binding properties of the complexes **1**, **3** and **6** to CT DNA in 50 mM Tris HCl/1 mM NaCl buffer, pH 7.5). Fluorescence intensities of EB at 610 nm with an excitation wavelength of 430 nm were measured at different complex concentrations. Reduction in the emission intensity was observed with addition of the complexes. The apparent binding constant (K_{app}) was calculated using the equation K_{EB}[EB]/K_{app}[complex], where the complex concentration was the value at a 50% reduction of the fluorescence intensity of EB and $K_{EB} = 1.0 \times 10^7$ M^{-1} ([EB] = 3.3 μM).[54]

Viscosity measurements were carried out using an Ostwald-type viscometer of 2 mL capacity, maintained at a constant temperature of 25.0 ± 0.1 °C in a thermostatic bath. DNA samples approximately 200 bp in length were prepared by sonication in order to minimize complexities arising from DNA flexibility.[55] The flow time was measured with a digital stopwatch, and each sample was tested three times to get an average calculated time. Data were presented as $(\eta/\eta_0)^{1/3}$ *vs.* binding ratio,[56] where η is the viscosity of DNA in the presence of complex, η_0 is the viscosity of free DNA.

Cyclic dichroic (CD) spectra of the CT DNA were measured using a JASCO J-715 spectropolarimeter equipped with a Peltier temperature control device at 25 ± 0.1 °C. All experiments were done using a quartz cell of 1 cm path length. Each CD spectrum was recorded after averaging over at least 5 accumulations using a scan speed of 100 nm min^{-1}.

DNA cleavage experiments

The cleavage of plasmid DNA was monitored by agarose gel electrophoresis. Supercoiled pBR322DNA (0.020 mg mL^{-1}) in 50 mM Tris-HCl/NaCl buffer (pH 7.2) was treated with the complexes **2**, **5** and **6** (30–50 μM) and H_2O_2 (40 μM). All the samples were incubated for 30 min at 37 °C followed by its addition to the loading buffer containing 25% bromophenol blue, 0.25% xylene cyanol, 30% glycerol (3 μL). All the samples were finally loaded on 0.8% agarose gel containing EB (1 μg mL^{-1}). Electrophoresis was carried out at 50 V for 1 h in TBE buffer (45 mM Tris, 45 mM H_3BO_3, 1 mM EDTA, pH 8.3). Resulting bands were visualized by UV light and photographed. DNA ligation experiments[43] as follows: after incubation of pBR322 DNA with **5** and **6** (50 μM) in the presence of hydrogen peroxide for 1 h at 37 °C, the cleavage product, *i.e.* linear form, was purified by DNA gel extraction kit. The linear DNA (2 μL) (nicked by Ni(II) complexes **5** and **6**) was incubated for 12 h at 16 °C with 1μL of T4 ligase (4 units) and 1 mM ATP containing ligation buffer (10 μL). Afterwards, the ligation products were electrophoresed, stained and imaged. Quantification was performed by fluorescence imaging by use of a Gel-Doc 1000 (BioRad) and data analysis with Multianalysis software (version 1.1).

Conclusions

Based on the electrochemical studies, the Ni(II) ion located in the alkyl oxime moiety, reduces at less negative potential than the Ni(II) ion present in the imine moiety. Phosphate hydrolysis studies show that the complex **1** has a higher catalytic activity than the other corresponding unsymmetrical binuclear Ni(II)

analogues. The DNA binding experiments results shows that the aromatic diimine containing Ni(II) complex **6** display better binding propensity with DNA than aliphatic diimine containing Ni(II) analogues **1** and **3**. All the complexes can cleave the DNA through hydrolytically, because a classical radical scavenger, such as dimethyl sulfoxide (DMSO), was completely ineffective in the cleavage activity.

Abbreviations

DMF	*N*,*N*-dimethylformamide
MES	2-(*N*-morpholino)ethanesulfonic acid
CHES	2-(Cyclohexylamino)ethanesulfonic acid
EB	Ethidium bromide
CT-DNA	Calf thymus DNA
Tris	Tris(hydroxymethyl)aminomethane
TBE	Tris-boric acid-EDTA
EDTA	Ethylenediaminetetraacetic acid
SOD	Superoxide dismutase

Acknowledgements

The authors thank the Department of Science and Technology (DST-FIST), New Delhi, Government of India, for financial support. Dr M. R. N. Murthy and Mr. M. Govindaraju, Molecular Biophysics Unit, Indian Institute of Science, Bangalore, India, are gratefully acknowledged for providing the Circular Dichroism Spectral facility. S. A. is grateful to CSIR (SRF), New Delhi, Government of India, for a fellowship.

References

1 (*a*) M. A. Halcrow and G. Christou, *Chem. Rev.*, 1994, **94**, 2421; (*b*) T. I. Doukov, T. M. Iverson, J. Seravalli, S. W. Ragsdale and C. L. Drennan, *Science*, 2002, **298**, 567.
2 (*a*) R. K. Andrews, R. L. Blakely and B. Zerner, *Adv. Inorg. Biochem.*, 1984, **6**, 245; (*b*) P. A. Clark and D. E. Wilcox, *Inorg. Chem.*, 1989, **28**, 1326; (*c*) B. S. Cooperman, *Met. Ions Biol. Syst.*, 1976, **5**, 79; (*d*) N. E. Dixon, P. W. Riddles, C. Gazzola, R. L. Blakely and B. Zerner, *Can. J. Biochem.*, 1980, **58**, 1335.
3 T. Koike and E. Kinuira, *J. Am. Chem. Soc.*, 1991, **113**, 8935.
4 N. Baskaran, V. Prakash, H. S. Savithri, A. N. Radhakrishnan and N. Appaji Rao, *Biochemistry*, 1989, **28**, 9613.
5 G. A. Rosenthal, *Life Sci.*, 1997, **60**, 1635.
6 K. Yamaguchi, F. Akagi, S. Fujinami, M. Suzuki, M. Shionoya and S. Suzuki, *Chem. Commun.*, 2001, 375.
7 P. R. Reddy and K. S. Rao, *Chem. Biodiversity*, 2006, **3**, 231.
8 C. J. Burrows and S. Rokita, *Acc. Chem. Res.*, 1994, **27**, 295.
9 J. G. Muller, X. Chen, A. C. Dadiz, S. E. Rokita and C. J. Burrows, *J. Am. Chem. Soc.*, 1992, **114**, 6407.
10 X. Chen, C. J. Burrows and S. E. Rokita, *J. Am. Chem. Soc.*, 1992, **114**, 322.
11 D. P. Mack and P. B. Dervan, *J. Am. Chem. Soc.*, 1990, **112**, 4604.
12 (*a*) H.-Y. Wang, W.-B. Yuan, Q. Zhang, S.-W. Chen and S.-S. Wu, *Transition Met. Chem.*, 2008, **33**, 593; (*b*) K. G. Ragunathan and H.-J. Schneider, *Angew. Chem., Int. Ed. Engl.*, 1996, **35**, 1219.
13 X. Chen, J. Wang, S. Sun, J. Fan, S. Wu, J. Liu, S. Ma, L. Zhang and X. Peng, *Bioorg. Med. Chem. Lett.*, 2008, **18**, 109.
14 O. Iranzo, A. Y. Kovalevsky, J. R. Morrow and J. P. Richard, *J. Am. Chem. Soc.*, 2003, **125**, 1988.
15 S. Anbu, M. Kandaswamy, P. Sudhakaran, V. Murugan and Babu Varghese, *J. Inorg. Biochem.*, 2009, **103**, 401.
16 S. Anbu, M. Kandaswamy and Babu Varghese, *Acta Crystallogr., Sect. E: Struct. Rep. Online*, 2007, **63**, m2330.
17 D. Volkmer, B. Hommerich, K. Griesar, W. Haase and B. Krebs, *Inorg. Chem.*, 1996, **35**, 3792.
18 M. Ciampolini, *Inorg. Chem.*, 1966, **5**, 35.
19 L. Sacconi, M. Ciampolini and G. P. Speroni, *J. Am. Chem. Soc.*, 1965, **87**, 3102.
20 S. Akine, T. Taniguchi and T. Nabeshima, *Chem. Lett.*, 2001, 682.
21 (*a*) M. M. Bhadbhade and D. Srinivas, *Inorg. Chem.*, 1993, **32**, 6122; (*b*) S. K. Mandal and K. Nag, *J. Chem. Soc., Dalton Trans.*, 1983, 2429.
22 W. E. Gao, G. Bu, D. Yang, Z. Liao, S. Jiang, G. Yan and J. Way, *J. Chem. Soc., Dalton Trans.*, 2000, 1431.
23 J. Manonmani, R. Thirumurugan, M. Kandaswamy, V. Narayanan, V. Shanmugasundara Raj, M. N. Ponnuswamy, G. Shanmugam and H. K. Fun, *Polyhedron*, 2001, **20**, 3039.
24 M. Thirumavalavan, P. Akilan and M. Kandaswamy, *Supramol. Chem.*, 2004, **16**, 495.
25 R. Das and K. Nag, *Inorg. Chem.*, 1991, **30**, 2833.
26 N. A. Rey, A. Neves, A. Bortoluzzi, C. T. Pich and H. Terenzi, *Inorg. Chem.*, 2007, **46**, 348.
27 M. Thirumavalavan, P. Akilan and M. Kandaswamy, *Polyhedron*, 2005, **24**, 1781.
28 N. Sengottuvelan, D. Saravanakumar and M. Kandaswamy, *Polyhedron*, 2007, **26**, 3825.
29 C. T. Yang, M. Vetrichelvan, X. Yang, B. Moubaraki, K. S. Murray and J. J. Vittal, *Dalton Trans.*, 2004, 113.
30 V. Uma, M. Kanthimathi, T. Weyhermuller and B. Unni Nair, *J. Inorg. Biochem.*, 2005, **99**, 2299.
31 B. Peng, H. Chao, B. Sun, H. Li, F. Gao and L.-N. Ji, *J. Inorg. Biochem.*, 2006, **100**, 1487.
32 P. K. Sasmal, A. K. Patra, M. Nethaji and A. R. Chakravarty, *Inorg. Chem.*, 2007, **46**, 11112.
33 E. Nyarko, N. Hanada, A. Habib and M. Tabata, *Inorg. Chim. Acta*, 2004, **357**, 739.
34 J. B. Lepecq and C. Paoletti, *J. Mol. Biol.*, 1967, **27**, 87.
35 M. Lee, A. L. Rhodes, M. D. Wyatt, S. Forrow and J. A. Hartley, *Biochemistry*, 1993, **32**, 4237.
36 W. Qian, F. Gu, L. Gao, S. Feng, D. Yan, D. Liao and P. Cheng, *Dalton Trans.*, 2007, 1060.
37 B. Peng, X. Chen, K.-J. Du, B.-L. Yu, H. Chao and L.-N. Ji, *Spectrochim. Acta, Part A*, 2009, **74**, 896.
38 (*a*) J.-Z. Wu, L. Yuan and J.-F. Wu, *J. Inorg. Biochem.*, 2005, **99**, 2211; (*b*) J. Talib, D. G. Harman, C. T. Dillon, J. A. Wright, J. L. Becka and S. F. Ralph, *Dalton Trans.*, 2009, 504.
39 J. He, J. Sun, Z.-W. Mao, L.-N. Ji and H. Sun, *J. Inorg. Biochem.*, 2009, **103**, 851.
40 V. I. Ivanov, L. E. Minchenkova, A. K. Schyolkina and A. I. Poletayer, *Biopolymers*, 1973, **12**, 89.
41 J. A. Cowan, *Curr. Opin. Chem. Biol.*, 2001, **5**, 634.
42 (*a*) A. Sreedhara and J. D. Cowan, *Chem. Commun.*, 1998, 1737; (*b*) S. Dhar, P. A. N. Reddy and A. R. Chakravarty, *Dalton Trans.*, 2004, 697.
43 C. Liu, S. Yu, D. Li, Z. Liao, X. Sun and H. Xu, *Inorg. Chem.*, 2002, **41**, 913.
44 L. M. T. Schnaith, R. S. Banson and L. Que Jr., *Proc. Natl. Acad. Sci. U. S. A.*, 1994, **91**, 569.
45 M. C. B. Oliveira, M. S. R. Couto, P. C. Severino, T. Foppa, G. T. S. Martins, B. Szpoganicz, R. A. Peralta, A. Neves and H. Terenzi, *Polyhedron*, 2005, **24**, 495.
46 N. V. Verani, E. Rentschler, T. Weyhermuller, E. Bill and P. Chaudhuri, *J. Chem. Soc., Dalton Trans.*, 2000, 251.
47 D. W. Dixon and R. H. Weiss, *J. Org. Chem.*, 1984, **49**, 4487.
48 M. Thirumavalavan, P. Akilan and M. Kandaswamy, *Inorg. Chem.*, 2003, **42**, 3308.
49 *Bruker-Nonius (2004). APEX-II and SAINT-Plus (version 7.06a)*, Bruker AXS Inc., Madison, Wisconsin, USA.
50 *SADABS*, Bruker AXS Inc., Madison, Wisconsin, USA.
51 A. Altormare, G. Gascarano, C. Giacovazzo and A. Guagliardi, (1993) SIR92, *J. Appl. Crystallogr.*, 1993, **26**, 343.
52 M. E. Reichmann, S. A. Rice, C. A. Thomas and P. Doty, *J. Am. Chem. Soc.*, 1954, **76**, 3047.
53 A. Wolfe, G. H. Shimer and T. Mechan, *Biochemistry*, 1987, **26**, 6392.
54 Y. Zhao, J. Zhu, W. He, Z. Yang, Y. Zhu, Y. Li, J. Zhang and Z. Guo, *Chem.–Eur. J.*, 2006, **12**, 6621.
55 J. B. Chaires, N. Dattagupta and D. M. Crothers, *Biochemistry*, 1982, **21**, 3933.
56 G. Cohen and H. Eisenberg, *Biopolymers*, 1969, **8**, 45.

